Advanced Real-Time Process Analytics for Multistep Synthesis in Continuous Flow

Peter Sagmeister,[a,b] René Lebl,[a,b] Ismael Castillo,[c] Jakob Rehrl,[d] Julia Kruisz,[d] Martin Sipek,[e] Martin Horn,[c] Stephan Sacher,[d] David Cantillo,[a,b] Jason D. Williams[a,b]* and C. Oliver Kappe[a,b]*

[a]Center for Continuous Flow Synthesis and Processing (CCFLOW), Research Center Pharmaceutical Engineering GmbH (RCPE), Inffeldgasse 13, Graz 8010, Austria

[b]Institute of Chemistry, University of Graz, NAWI Graz, Heinrichstrasse 28, Graz 8010, Austria

[c]Institute of Automation and Control, Graz University of Technology, Inffeldgasse 21b, Graz 8010, Austria

[d]Research Center Pharmaceutical Engineering (RCPE), Inffeldgasse 13, Graz 8010, Austria

[e]Evon GmbH, Wollsdorf 154, St. Ruprecht a. d. Raab 8181, Austria

*E-mail: jason.williams@rcpe.at; oliver.kappe@uni-graz.at

Supporting information for this article is available online

Abstract: In multistep continuous flow chemistry, studying complex reaction mixtures in real time is a significant challenge, but provides an opportunity to enhance reaction understanding and control. We report the integration of four orthogonal Process Analytical Technology tools (NMR, UV/vis, IR and UHPLC) in the multistep synthesis of an Active Pharmaceutical Ingredient, mesalazine. This synthetic route makes optimal use of flow processing for nitration, high temperature hydrolysis and hydrogenation steps, as well as three inline separations. Advanced data analysis models were developed (indirect hard modelling, deep learning and partial least squares regression), to quantify the desired products, intermediates and impurities in real time, at multiple points along the synthetic pathway. The capabilities of the system have been demonstrated by operating both steady state and dynamic experiments and represents a significant step forward in data-driven continuous flow synthesis.

Introduction

Continuous flow processing is now widely accepted as a disruptive technology in the synthesis of Active Pharmaceutical Ingredients (APIs) as well as other fine and commodity chemicals.[1] Its impact is particularly noteworthy in the operation of multiple synthetic transformations in sequence, known as multistep flow synthesis. A number of APIs have been synthesized using this approach, stringing together numerous reaction steps, often providing significant improvements in processing time, safety and yield.[2] As the chemical industries move towards increased digitization in development and manufacturing, establishing data-rich multistep synthesis is of prime importance.[3]

Process Analytical Technology (PAT)[4] now plays an increasingly central role in continuous flow processing.[5] Real-time reaction monitoring has been invoked for a range of applications, such as self-optimization,[6] reaction kinetic analysis,[7] dynamic experimentation,[8] online chiral analysis[9] and process control.[10] In particular, there is clear support from regulatory agencies within the pharmaceutical industry for the incorporation of PAT in continuous manufacturing processes to ensure a high standard of safety and product quality.[11]

Generally, where these instruments are utilized, only relatively simplistic data processing is used to determine reaction progress, or relative product distribution (i.e. % content). However, when combined with powerful data processing techniques, these tools can be used to precisely discern the *concentration* of products and impurities present, which gives a substantially better overview for process control, especially where intermediate workup/separation steps are concerned. This is an important challenge in the context of complex reaction mixtures with numerous overlapping species

The combination of multistep flow synthesis with multiple PAT tools is an area in which surprisingly little work has been disseminated. A recent report from our laboratories detailed the basic use of three separate PAT tools in an organometallic reaction.[12] Based on this experience, we endeavored to expand to a more integrated reaction and analytics platform, monitored and controlled by a single computer program. The system should be capable of communicating with all process peripherals (PAT tools, pumps, sensors, thermostats, mass flow controllers etc.). Implementing multiple orthogonal analytical techniques is expected to open new possibilities in reaction understanding, optimization and process control. This is especially true in cases which allow the data from one instrument to be used in synergy with other instruments, to validate results or to improve quantification performance, owing to some level of redundancy.

In order to exemplify this system, the synthesis of mesalazine (**5-ASA**), a commonly used drug for the treatment of Crohn's disease and colitis, was targeted.[13] The proposed synthetic route (**Scheme 1a**) begins from 2-chlorobenzoic acid

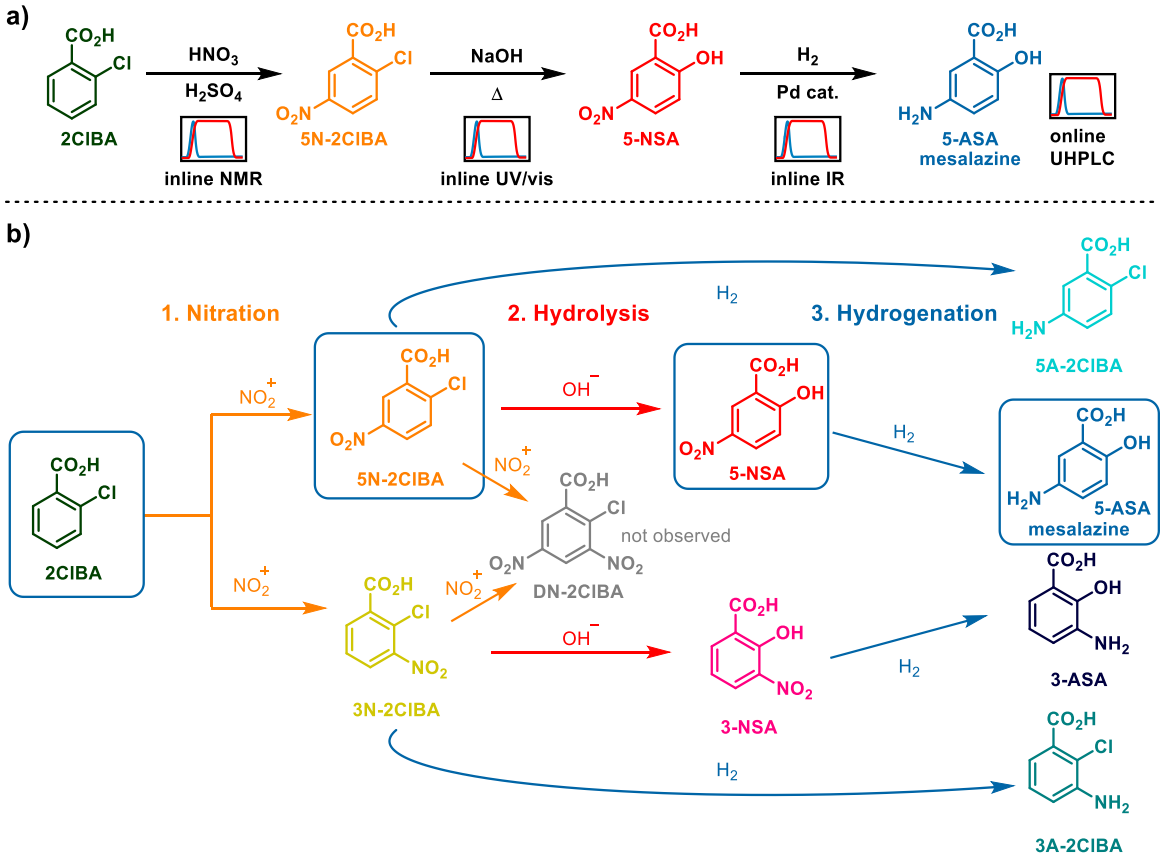

Figure 1. a) The proposed synthetic route for the synthesis of mesalazine (**5-ASA**) from 2-chlorobenzoic acid (**2ClBA**), via a 3-step synthetic process. Each step will be analyzed in real-time using a different PAT tool, as well as a final analysis by UHPLC. **b)** Impurity map, showing the main expected impurities in this multistep process. Intermediates along the desired reaction pathway are depicted in a blue box.

(**2ClBA**), which is nitrated (hazardous chemistry)[1] to provide 5-nitro-2-chlorobenzoic acid (**5N-2ClBA**) as the major isomer. The aryl chloride is then displaced by hydroxide at a temperature above the solvent boiling point (extreme process windows),[14] yielding 5-nitrosalicylic acid (**5-NSA**). A final hydrogenation step using catalytic static mixers (CSMs,[15] gas-liquid chemistry)[16] furnishes the API, mesalazine (**5-ASA**). The nitration is monitored by NMR, then hydrolysis by UV/vis and, finally, hydrogenation is monitored by IR, with a final quantification by UHPLC. The flow process must integrate a quench of the nitrating mixture, along with two phase separations, facilitating an acid-base extraction for the following hydrolysis step. The expected impurities in this sequence, owing to incomplete conversion, or overreaction (**Figure 1b**) have been considered for analysis and quantification after each reaction step.

Here we report the development of a multistep continuous flow platform for the synthesis of mesalazine. The implemented PAT strategy employs three different advanced data analysis methods and is capable of quantifying numerous species (including intermediates and impurities) at different points along the process. To our knowledge, such a level of PAT integration in continuous flow synthesis has not before been reported and leads towards a strong level of process understanding and control.

Results and Discussion

Nitration and Acid/base Extraction

The first step in the synthetic route is the nitration of **2ClBA**. Although nitration reactions are a prime example of hazardous chemistry benefiting from continuous flow processing, there are a relatively small number of cases where these are employed in multistep sequences.[17] It is assumed that this is due to the large amount of water necessary to dilute the reaction medium (often sulfuric acid), which requires a phase separation. Considering the large volume of aqueous medium, this is perhaps best performed using a gravity separation, or counter-current extraction.[18] However, for a small scale lab process, these techniques are impracticable, due to their relatively large volumes. Instead, we opted to employ membrane separation as a simple, small volume separation solution.[19]

Initial work was conducted using the highly reactive salicylic acid, but poor regioselectivity was achieved and a significant quantity of overreaction was observed.[20] To combat this issue, the starting material was replaced with **2ClBA** and a hydrolysis step was added afterward (**Figure 1a**). Due to the high viscosity of the sulfuric acid solvent and relatively low flow rates (~1 mL/min combined) a split-and-recombine type mixer (Ehrfeld, Cascade mixer) was required to achieve sufficient mixing for effective reaction (**Figure 2a**).[21]

Following the reaction itself, a quench/extraction was performed by combining the reaction stream with a premixed water/isopropyl acetate (iPrOAc) stream. To control the exothermic dilution of sulfuric acid, and ensure efficient extraction, this was performed in a microstructured reactor (Ehrfeld, FlowPlate, L/L process plate), optimized for biphasic mixing.[22] Since the dilution of sulfuric acid at this point is critical for a safe quench and effective phase separation, a ratio of water to sulfuric acid flow rates was maintained above 5.5 during optimization and long term processing.

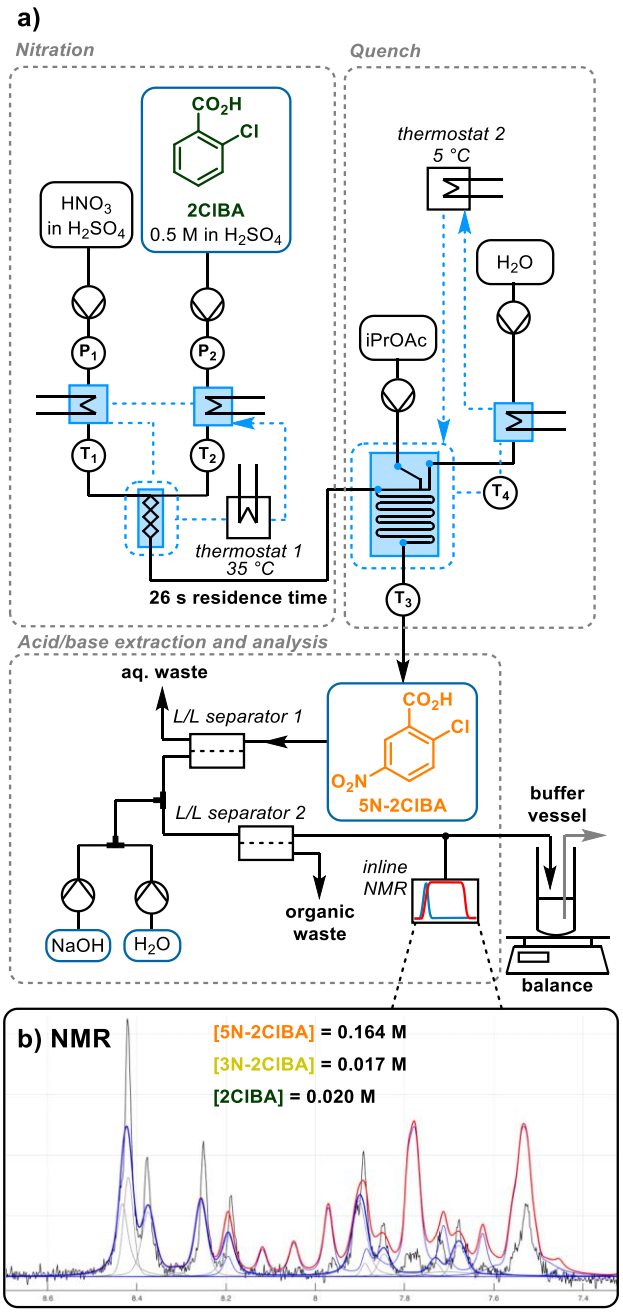

Figure 2. a) Detailed schematic diagram of the nitration reaction step, followed by aqueous quench and acid/base extraction using membrane separators. T and P represent temperature and pressure sensors, respectively. **b)** An example process NMR spectrum showing: the recorded low field spectrum (black), the **5N-2CIBA** model (dark blue), the IHM component mixture model (red), with its component individual peaks (gray).

To determine the ideal operating space for the nitration reaction, a detailed study was carried out examining the effect of flow rate, temperature and HNO_3 stoichiometry. Although overnitration (producing **DN-2CIBA**, **Figure 1b**) was not observed, valuable knowledge around regioselectivity was obtained. An operating range for complete **2CIBA** conversion, but <15% **3N-2CIBA** was defined, around the experimental point: 26 s residence time, 35 °C, 1.6 equiv HNO_3. Furthermore, the reaction progress over time was examined, clearly showing the reaction progress between 3.4 s and 20.6 s residence time, at three different temperatures.

Since the hydrolysis step requires basic conditions, an acid/base extraction was implemented, using two membrane-based separators (Zaiput, SEP-10). First, the acidic aqueous layer was separated from the iPrOAc layer, which contained the organic products. This organic stream was then mixed with sodium hydroxide to deprotonate the carboxylic acid moieties and allow extraction back into the aqueous layer. A second membrane unit separated the basic aqueous phase for onward reaction.

The performance of this nitration and acid/base extraction sequence was analyzed using inline NMR (Magritek, Spinsolve Ultra 43 MHz), generating a ^{1}H NMR spectrum every 12 s. Because of numerous overlapping peaks, simple peak integration was not feasible, so an Indirect Hard Modelling (IHM) approach to quantification was used (**Figure 2b**).[23] This approach fits Gaussian/Lorentzian peaks to the NMR signals to build a chemometric model, which permits flexibility for small changes in peak positions and shapes (S-PACT, PEAXACT software). The resulting model facilitated accurate component quantification from process spectra (see SI for details).

By this approach, it was possible to quantify the concentration of each of the three reaction species at this point (**2CIBA**, **5N-2CIBA** and **3N-2CIBA**), achieving an error of 2.4, 3.3 and 3.8 mM for the starting material **2CIBA**, desired product **5N-2CIBA** and regioisomer **3N-2CIBA**, respectively (error of validation, see SI for details). The combined analyte concentration at this point was ~200 mM, so these values represent an excellent model for quantifying the major species. Under normal operation, the concentrations of **2CIBA** and **3N-2CIBA** are expected to be far lower (in the region of 10-20 mM, **Figure 2b**), but the models certainly remain accurate enough to monitor trends and process deviations. Due to occasional spikes in the data (thought to be caused by gas bubbles) a filter was applied, which removed values outside of a 5 standard deviation range, based on the previous five data points.

Upon further consideration of the NMR data, it was found to be possible to quantify the hydroxide concentration. A linear relationship between hydroxide concentration and the chemical shift of the water peak was found (using the isopropyl acetate as a reference point, see SI for details). During an early long run experiment (first two reaction steps, see SI), a lower-than-expected concentration of hydroxide reached the second reaction step. This was attributed to the carry-over of acid from the first separation, leading to partial neutralization.

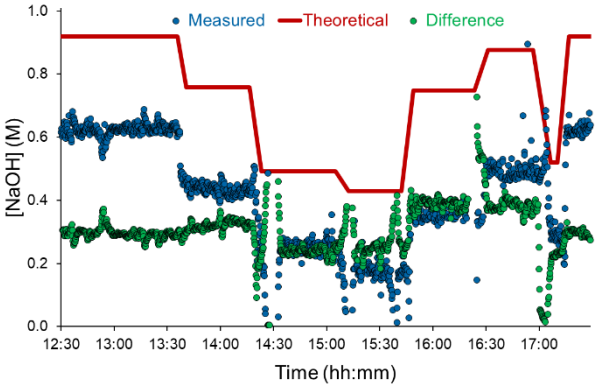

Figure 3. A graph showing the determination of hydroxide concentration by NMR, and multiple different pump set points. The measured concentration is shown in blue points, whilst the theoretical (expected) concentration is shown as a red line. The difference between the two is represented in green.

Using this calibration, the quantity of acid leaching through the separator could be estimated, by taking the difference between the expected and observed concentration of NaOH (note that this also had to be corrected for substrate concentrations, due to their carboxylic acid moieties). The quantity of H_2SO_4 dissolved in iPrOAc and carried through the separator was estimated to be in the range of 0.3 M, but varied depending on the flow rates and reaction conditions used (**Figure 3**). In response to this discrepancy, the input concentration of NaOH can be controlled in real time (whilst maintaining a constant flow rate) by the two pumps positioned after L/L separator 1 (**Figure 2a**). It should be noted that some retention of iPrOAc at L/L separator 2 was also observed and quantified by the same IHM.

Hydrolysis

In order to install the necessary hydroxyl group, hydrolysis of the aryl chloride intermediate **5N-2ClBA** was performed in a stainless steel coil at elevated temperature, up to 210 °C. This facilitated complete conversion in residence times as short as 5 min. To operate at elevated temperature, the reactor required pressurization, where previously no back pressure was applied. To solve this, two separate pressure zones were set up by using a buffer (or holdup) vessel to feed an HPLC pump (**Figure 4a**).

To take into account varying flow rates in the overall process, this buffer vessel was positioned on a balance. The balance and HPLC pump were integrated in a control loop, which adjusted the pump flow rate to keep the mass of process medium in the buffer vessel constant at 4 g. Due to the varying flow rates, different residence times were experienced in the hydrolysis step. Accordingly, a detailed time course study was carried out to ensure that reaction completion would be achieved, even at shorter residence times. To build up a detailed operating window, temperature and equivalents of NaOH were also varied (see SI).

At the hydrolysis reactor outlet, the extent of conversion was monitored using UV/vis spectrometry. In order to avoid compatibility issues with the pressurized and high pH reaction medium, a home-made flow cell was constructed. The probe was positioned in contact with the PFA tubing containing the reaction stream (0.8 mm inner diameter) held within a PEEK 4-way connector (see SI). Due to the high absorbance of this reaction mixture, a reflectance probe was used, since standard absorbance measurements were saturated.

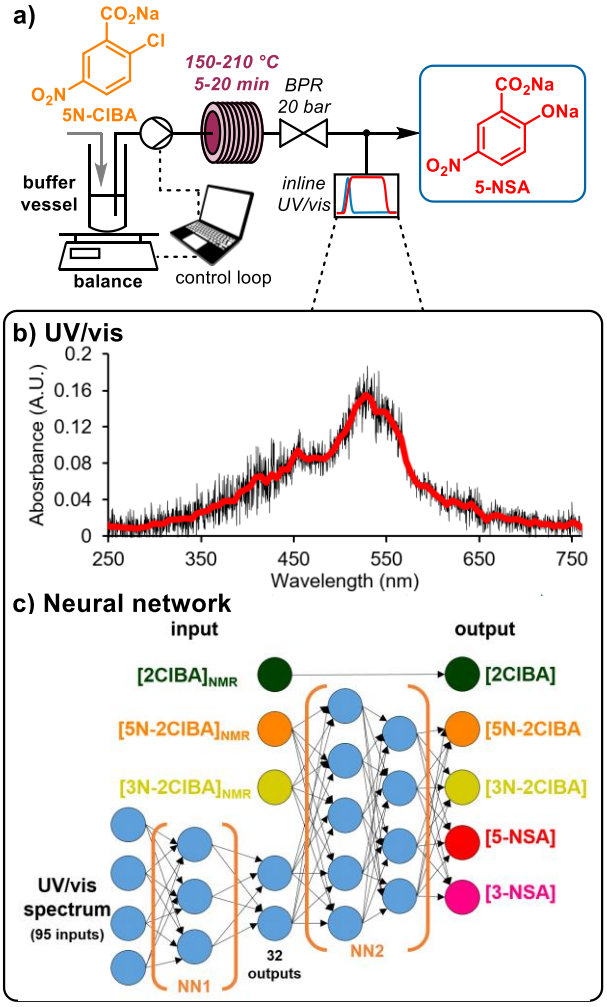

Figure 4. a) Detailed schematic diagram of the hydrolysis reaction step, using a heated coil reactor. The reactor output is analyzed by UV/vis. **b)** Example UV/vis spectrum, which shows no distinct spectral features for individual species quantification. **c)** A schematic diagram of the composed neural networks, which take the UV/vis spectrum and input concentrations (determined by NMR in the previous step), to provide concentrations of the five reaction components at this point.

The spectra collected at this point, every 2 s, showed relatively little in the way of spectral features (**Figure 4b**), therefore it was decided to implement a neural network (NN) to quantify analytes (**Figure 4c**).[24] To our knowledge, the use of deep learning to real-time PAT data for organic synthesis in continuous flow has not before been described,[25] but holds significant promise, particularly when amalgamated with knowledge from other instruments. The developed NNs functioned by combining the UV/vis spectrum with previously measured NMR data to determine the analyte concentrations at this point. In order to simplify the NN input, the UV/vis spectrum was reduced from 2048 data points to 95, by averaging every 20 values (roughly 5-6 nm). This was then processed by NN1, resulting in 32 outputs. These were combined with concentrations previously measured at the NMR, for interpretation by NN2.

NMR results were smoothed using a Savitzky-Golay filter (window of 25 spectra with 3rd order polynomial treatment) and fed forward by the difference in residence time between the two instruments (~20 min). **2ClBA** was not observed to undergo any

reaction in the hydrolysis step, so its previously measured concentration was simply read out as the current concentration. The other two concentrations from the NMR were fed into NN2, along with the UV/vis spectrum (represented by 32 data points), which provided concentrations of all four remaining species.

The NNs were scripted in python (v3.7), using Keras application programming interface (based on TensorFlow 2.0). Training was done using data obtained by ramping the temperature of the hydrolysis reactor from 20 °C to 210 °C, to provide 0-100% conversion of the input material (~35 000 spectra). These were augmented with compound mixture spectra (~8 000 spectra) and selected steady state levels from pre-existing process data (~6 000 spectra). The "Adam" optimizer was used and 25% of the data was removed to use as a validation subset. Resulting error statistics were very low (e.g. desired product **5-NSA** = 2.8 mM), but it should be noted that these values will also be impacted by errors propagated from the NMR quantification model.

Hydrogenation

The final synthetic transformation is the reduction of the installed nitro group to its corresponding amine (**Figure 5a**). Nitro reductions have become a routine reaction for operation under continuous flow conditions, generally using a packed bed reactor.[26] However, recent advances in 3D printing and coating technologies have introduced catalytically-coated static mixers (CSMs) as a viable alternative.[15] This approach facilitates simplified scale-up, since particle sizing, channeling and pressure drop issues can be obviated. For this multistep process, the hydrogenation was carried out using a reactor with rectangular channels with bespoke Pd electroplated CSMs inserted (Ehrfeld, Miprowa).

Hydrogen gas was supplied by a commercial H_2 generator with an integrated mass flow controller (Thales Nano, H-Genie) and the pressure was controlled by a back pressure regulator (Equilibar, Zero Flow) linked to a pressurized nitrogen supply, with automated electronic regulation (Bronkhorst, EL-PRESS). This setup facilitated reaction optimization, including automated adjustment of gas and liquid flow rates, system pressure and temperature. A study was also carried out for this reaction step, to provide a clear view of the influence of each reaction parameter and develop a robust operating space.

This study simply examined the conversion of **5-NSA** to **5-ASA**, with the assumption that the observed factor influences could be applied to other nitro compounds present in a telescoped process mixture. Aside from residence time, a high temperature (40-80 °C examined) was found to have the most significant influence, followed by the flow rate of H_2 (25-75 mL*N*/min examined). A high pressure (6-12 bar examined) was also found to help push the reaction to complete conversion, and numerous parameter interactions were also identified. It was extrapolated from this data that, when working at 80 °C and 12 bar pressure, all nitro species present in the reaction stream would be reduced to their corresponding anilines.

In order to provide online quantification of this step, a simple gas-liquid separator was constructed (see SI), leading to an IR probe (Mettler Toledo, ReactIR 15). Here, a spectrum was acquired every 15 s and the data was processed using a partial least squares (PLS) regression model.[20] This model was selected instead of an IHM in this case, due to better performance, but was also set up and processed in real time using PEAXACT software.

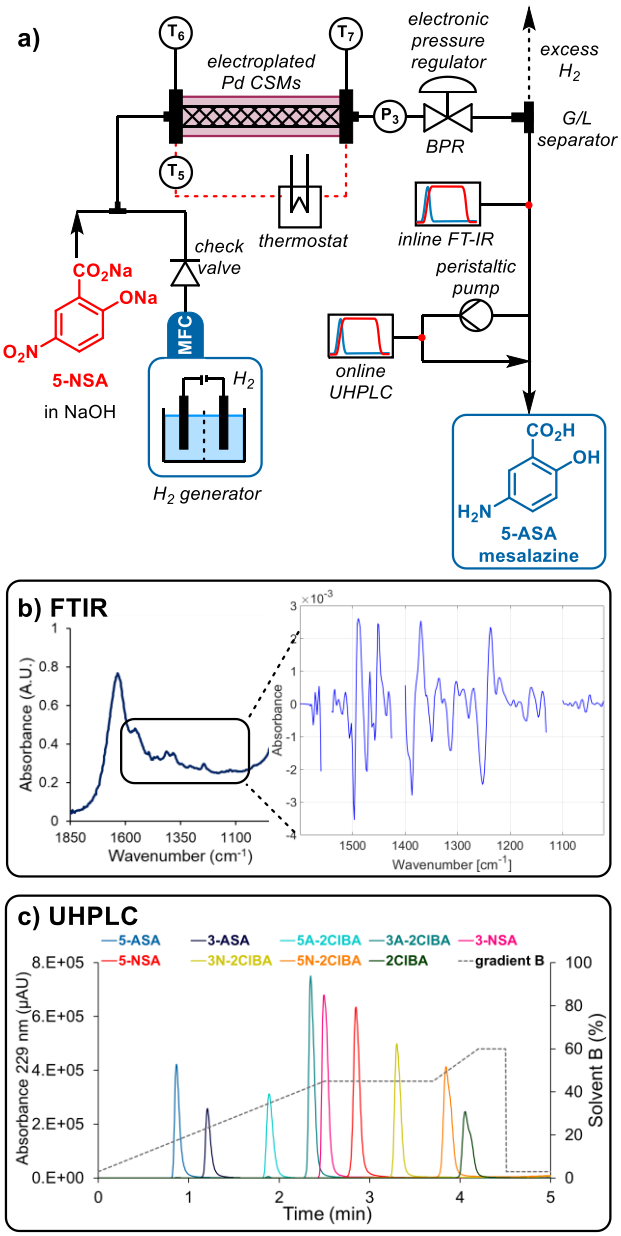

Figure 5. Schematic representation of the reaction and analytics setup used for the hydrogenation reaction. **a)** Detailed reaction setup schematic (P and T = pressure and temperature sensors). **b)** Representative infrared spectrum used for species quantification with a PLS model. The region considered is highlighted, with the insert showing the pretreated spectrum fed into the model. **c)** A demonstration of the species separation achieved in the developed online UHPLC method. The solvent gradient is plotted as a dotted line (gray). Note: an additional 2.5 min is allowed (not shown) for equilibration, prior to the next injection.

The model was trained for all nine components simultaneously, using seven mixture samples, along with two sets of process background spectra and one representative level from pre-existing process data. In this case, the individual component spectra were found to be detrimental to the model training, likely due to small spectral shifts caused by interactions between the components.

All component species had signals almost exclusively in the range of 1600-1020 cm^{-1}, with significant degree of overlap (**Figure 5b**). To further complicate matters, some isopropyl acetate (or its hydrolysis product, acetic acid) from the nitration reaction was still present, which also overlapped with analyte signals. In this instance, the correct pretreatment was key to a successful model. The spectral range was reduced to 1600-1020 cm^{-1}, a "rubberband" baseline correction was applied, as well as a first derivative transformation. For each component, non-contributing regions were also removed, as well as regions showing isopropyl acetate signals.

The models were validated using 10 separate averaged spectra from process data. Here, the errors were found to be low, considering the difficulty of quantification. The main product **5-ASA** was evaluated to have a validation error of 7.7 mM, which is <5% of the expected 180 mM concentration in the process stream. The models for other analytes provided validation errors of between 1.4 and 15.4 mM, implying overall excellent quantification accuracy. Furthermore, the variation between measurements was found to be very low, so no additional filter/averaging of the data was required. This set of PLS models provided useful concentration predictions for all nine of the examined species.

To achieve a detailed overview of the final reaction composition after the multistep procedure, online ultra high performance liquid chromatography (UHPLC, Shimadzu, Nexera X2) was incorporated, using a 10 nL sample injector (Vici, Cheminert Nanovolume). A fast gradient-based method was developed, which allowed an injection every 7.5 min (**Figure 5c**). Despite this short analysis time, all nine of the identified process components could be separated, allowing precise quantification. Again, all nine components were calibrated simultaneously, using seven injection mixtures of different concentration levels.

After optimization of the individual reaction steps, these were brought together to run as a telescoped process (**Figure 6**). Integration of all component parts within the same operational system was key to the smooth operation and management of this multistep process and its acquired data. This was achieved using Open Platform Communication Unified Architecture (OPC UA), a modern industry standard for inter-platform equipment communication. By this protocol, all pumps, probes, thermostats and other equipment were actively monitored and controlled through a single Supervisory Control And Data Acquisition (SCADA) software (Evon, XAMcontrol). Achieving this with equipment from numerous different suppliers represents a significant challenge, due to the lack of unified communication protocols and documentation. However, this also allowed real-time readouts of concentrations from the PAT tools, using the developed chemometric models. It should be noted that UHPLC and UV/vis results were delivered by a direct connection to the computer rather than OPC UA, with report file monitoring for new results (UHPLC) or a direct connection to the SCADA software (UV/vis).

To demonstrate the developed multistep process, a long run experiment at the developed optimal conditions was carried out for 3.5 h of steady state operation (**Figure 7**). The startup period in this case was of particular interest, since it demonstrates the distribution of the species as they progress through the system and reach each of the respective PAT instruments (**Figure 7a**). Steady state concentration was reached at the NMR after 22 min, UV/vis after 38 min and IR after 54 min. The use of analytical instruments with fast scan rates allow this characterization to be carried out in a straightforward manner, whilst preserving the reaction media viscosity and separation properties, since a different tracer reagent is not necessary.

Telescoped process: Steady State Operation

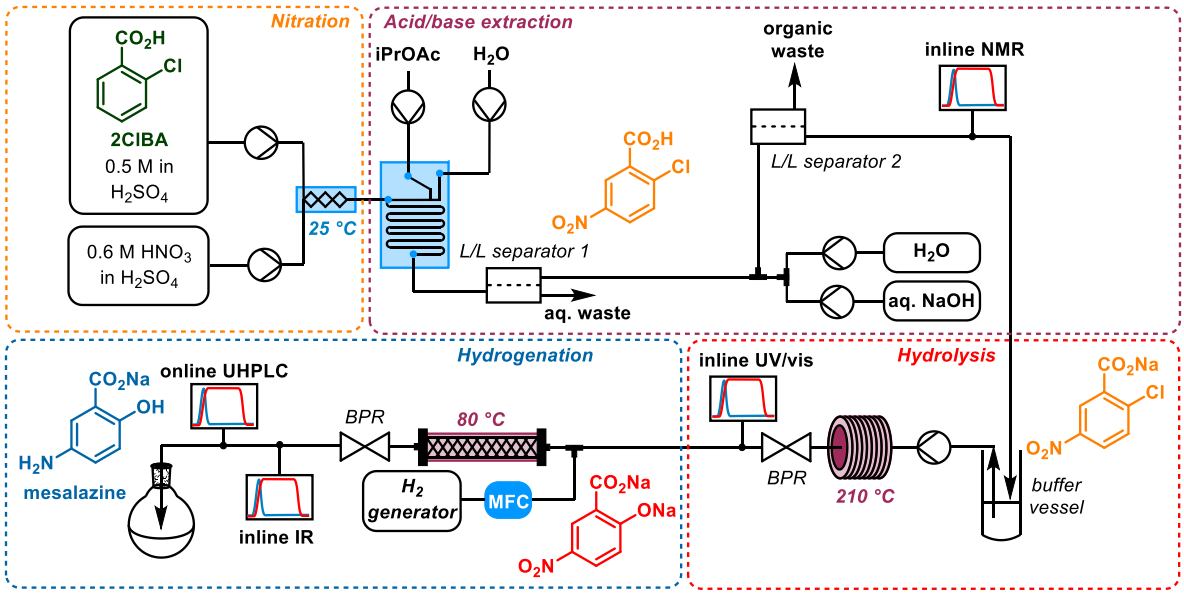

Figure 6. Schematic overview of the multistep, multi-PAT reaction setup towards the API mesalazine, **5-ASA**. For a more detailed overview, see SI

Another important aspect is the relative gradient of concentration increase at each point during the startup, which can be taken as a measure of flow dispersion. It would be expected that this gradient would become increasingly shallow as the time within the system increases, due to a broadening residence time distribution. The buffer vessel before the hydrolysis was of key concern here, but owing to the intentionally small holdup volume (~ 4 mL), this appears to have a minimal effect. This is evidenced by the comparable concentration gradients for the NMR, UV/vis and IR analyses. This relatively narrow distribution (i.e. good overall plug flow character) implies that the effect of parameter alterations should proliferate through the system quickly, without delay caused by excessive dead volume.

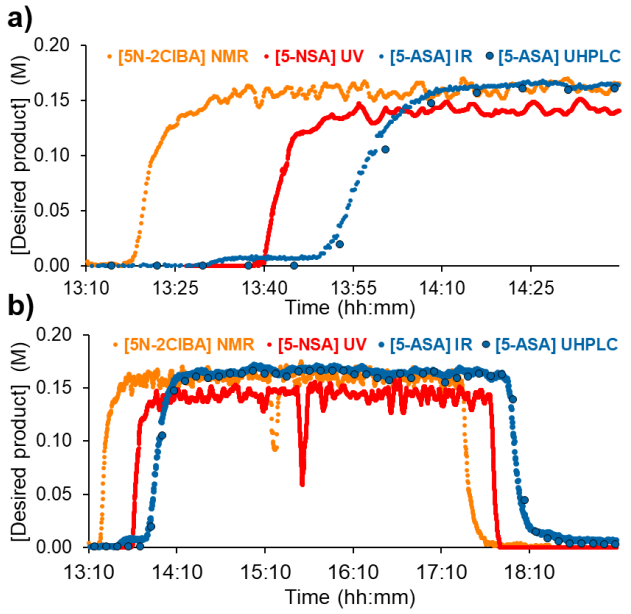

Figure 7. Graphs showing the steady state operation of the telescoped process. Note: for clarity, only the major species at each PAT tool is shown. **a)** An expanded section showing the process startup, to focus on the relative residence times and concentration gradients at each PAT tool. **b)** An overall view of the telescoped process. Note: the NMR shim was lost at 15:14, resulting in the observed concentration drop by both NMR and UV/vis analysis.

Once steady state was reached, processing was stable for the entire period, aside from a loss of NMR shim at 15:14 (**Figure 7**), which was observed by a drop in **[5N-2ClBA]** at the NMR. This could quickly be resolved by using a 6-port valve setup to inject a separate shim sample, resulting in recovery of steady state analysis within 6 min, without interfering with the process stream (15:14-15:20, **Figure 7**, see SI for details of 6-port valve setup). Because the UV/vis NN takes inputs from the NMR, this meant that the deviation was also observed in this instrument. However, the process stream would not erroneously be diverted to waste, since the disturbance was not observed by IR or UHPLC.

The steady state operation in this long run resulted in average **[5-ASA]** of 0.166 mM and average flow rate of 1.073 mL/min, synthesizing 1.6 g/h of the desired **5-ASA** product (mesalazine). This corresponds to 79% assay yield over three steps, based on input **2ClBA**. Extrapolating to longer term operation, this would provide 38.4 g per day in this lab scale system (total volume ~55 mL). It is envisaged that a larger scale system could be established in a facile manner, based on the rigorous reaction development performed here.

Telescoped process: Dynamic Operation

To demonstrate the synergy between different PAT tools and their predictive power towards rapidly detecting and monitoring process deviations, dynamic experimentation was carried out. This was performed by varying reaction temperatures within the ranges explored in the respective studies for each individual reaction step: 0-35 °C for nitration, 150-210 °C for hydrolysis and 40-80 °C for hydrogenation. The reactor temperature ramps were introduced separately, inducing changes in conversion and/or selectivity (**Figure 8**).

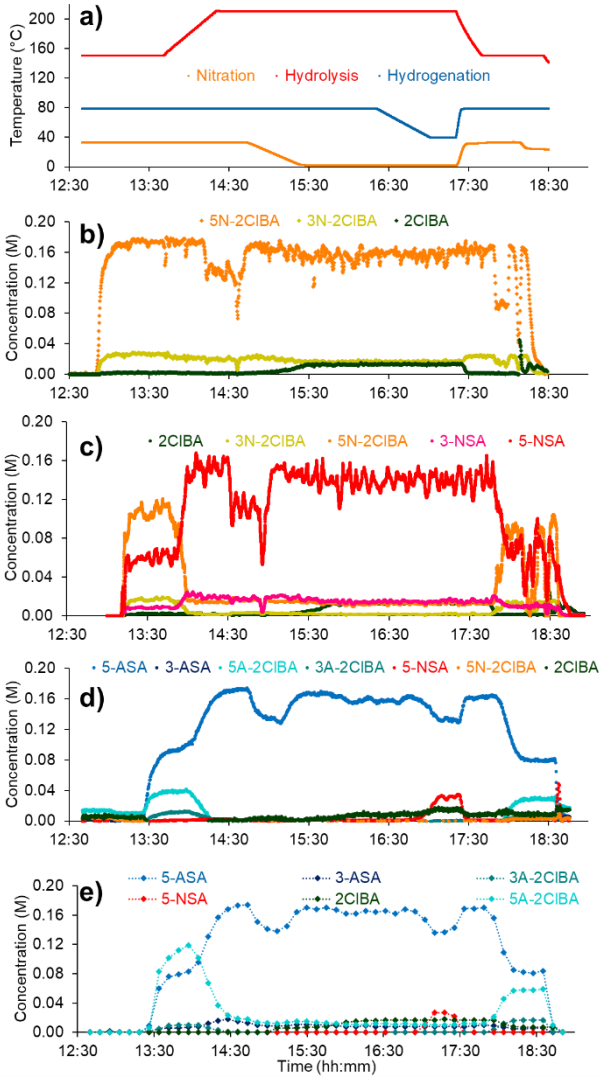

Figure 8. Summary of data from dynamic experiment, where temperatures of different reaction steps were varied. **a)** Temperature traces from the reactor, showing when changes were introduced. **b)** Inline NMR data, quantified by an indirect hard model. **c)** Inline UV/vis data, quantified by a neural network. **d**) Inline IR data, quantified by a partial least squares regression model. **e)** Online UHPLC data, quantified by peak integration.

Initially, a low temperature was set for the hydrolysis reaction (until 13:40), resulting in incomplete conversion and elevated **[5A-2ClBA]**, observed by IR and UHPLC. At this point,

one limitation of the IR PLS model is visible, since **[5A-2ClBA]** is estimated to be 40 mM, but online UHPLC analysis reveals concentration between 80-120 mM in the same region. Nevertheless, the correct trend is observed, which would allow correction of the reaction conditions, towards **5-ASA**, in a timely manner.

Prior to the decrease in nitration temperature, at 14:10 (**Figure 8**), a problem with L/L separator 1 was observed, characterized by a decrease in **[5N-2ClBA]** at the NMR. The quantification of concentration at this point, rather than relative product distribution, allowed the problem to be identified and solved quickly, by replacing the separator. This minimized the disruption caused, resulting in a drop of **[5-ASA]** at the UHPLC by ~40 mM for around 30 min.

At 14:45, the nitration temperature was decreased, resulting in incomplete conversion, with ~12-18 mM **2ClBA** remaining in the reaction mixture. This persisted through the process and was successfully quantified by all four PAT tools. Before increasing the nitration temperature to its original value, the hydrogenation temperature was also decreased (at 16:20). The effect was observed as an increase in nitro species, **5-NSA**, which was successfully detected at ~30 mM by both UHPLC and IR analyses. These results successfully demonstrate the utility of a multi-PAT approach for dynamic experimentation in a multistep system.

Conclusion

In summary, advanced analytical methods have been exemplified in a challenging multistep, multi-PAT synthetic sequence in flow, combining three synthetic steps and three phase separations. Three inline PAT tools were employed, each using a distinct data processing technique, followed by a final concentration confirmation by online UHPLC. Individual optimization of each step was carried out with onward compatibility in mind, establishing design space based on feasible and compatible parameter ranges. In parallel, chemometric models for the respective steps were also developed, using IHM for NMR, NNs for UV/vis and PLS for IR analyses. These models were integrated to the control software, providing real-time concentration data of up to nine different process species, with excellent accuracy overall.

Once the entire system had been combined, it was possible to implement the developed conditions with relatively little difficulty, facilitating stable operation. Of particular note, problems with phase separation were detected early on, allowing correction before the deviation had a significant effect. Furthermore, synergy between multiple PAT instruments has the capacity to improve chemometric models in two ways. Firstly, UHPLC quantification, can be used to add process data at steady state to training data sets for other PAT chemometric models. Additionally, as demonstrated with the UV/vis NN, analysis methods can be developed, which take previous measurements into account, in a feed-forward mechanism, enhancing the knowledge gained from data that would otherwise be difficult to interpret.

Mesalazine was synthesized in a fully controlled and robust manner, with a throughput of 1.6 g/h. The analytical power for determining process intermediates in real time was exemplified in a dynamic experiment, where relatively low concentrations (~10-30 mM) were quantified with good levels of accuracy. It is anticipated that the level of PAT integration demonstrated here will set a new precedent for analysis of multistep reactions in flow. Ongoing work in our labs will further capitalize on these developments in self-optimization and model-predictive control applications.

Acknowledgements

This work was funded by the Austrian Research Promotion Agency FFG No. 871458, within the program “Produktion der Zukunft”. The INFRA FLOW project (Zukunftsfonds Steiermark No. 9003) is funded by the State of Styria (Styrian Funding Agency SFG). The CCFLOW Project (Austrian Research Promotion Agency FFG No. 862766) is funded through the Austrian COMET Program by the Austrian Federal Ministry of Transport, Innovation and Technology (BMVIT), the Austrian Federal Ministry for Digital and Economic Affairs (BMDW), and by the State of Styria (Styrian Funding Agency SFG). The authors would like to thank Dr. Clemens Minnich and Dr Simon Kern (S-PACT) for software and chemometric model support, Dr. Stefan Kowarik (University of Graz) for assistance with neural networks and Mr Bernd Stein (HiTec Zang) for LabManager connectivity support.

Keywords: Flow chemistry • multistep synthesis • process analytical technologies • real-time analysis • process control

1. For reviews of flow chemistry for API synthesis, see: a) M. B. Plutschack, B. Pieber, K. Gilmore, P. H. Seeberger, *Chem. Rev.* **2017**, *117*, 11796–11893; b) R. Porta, M. Benaglia, A. Puglisi, *Org. Process Res. Dev.* **2016**, *20*, 2–25; c) B. Gutmann, D. Cantillo, C. O. Kappe, *Angew. Chem. Int. Ed.* **2015**, *54*, 6688–6728; d) R. Gérardy, N. Emmanuel, T. Toupy, V. E. Kassin, N. N. Tshibalonza, M. Schmitz, J. C. M. Monbaliu, *Eur. J. Org. Chem.* **2018**, *2018*, 2301–2351; e) S. Kobayashi, *Chem. Asian J.* **2016**, *11*, 425–436; e) M. Baumann, I. R. Baxendale, *Beilstein J. Org. Chem.* **2015**, *11*, 1194–1219.
2. For reviews of multistep flow synthesis, see: a) V. R. L. J. Bloemendal, M. A. C. H. Janssen, J. C. M. van Hest, F. P. J. T. Rutjes, *React. Chem. Eng.* **2020**, *5*, 1186–1197; b) Z. Fülöp, P. Szemesi, P. Bana, J. Éles, I. Greiner, *React. Chem. Eng.* **2020**, *5*, 1527–1555; c) J. Jiao, W. Nie, T. Yu, F. Yang, Q. Zhang, F. Aihemaiti, T. Yang, X. Liu, J. Wang, P. Li, *Chem. Eur. J.* **2020**, DOI 10.1002/chem.202004477.; d) J. Britton, C. L. Raston, *Chem. Soc. Rev.* **2017**, *46*, 1250–1271; e) D. Webb, T. F. Jamison, *Chem. Sci.* **2010**, *1*, 675–680; f) B. Pieber, K. Gilmore, P. H. Seeberger, *J. Flow Chem.* **2017**, *7*, 129–136.
3. For selected examples of integrated multistep flow systems, see: a) A. Adamo, R. L. Beingessner, M. Behnam, J. Chen, T. F. Jamison, K. F. Jensen, J. C. M. Monbaliu, A. S. Myerson, E. M. Revalor, D. R. Snead, T. Stelzer, N. Weeranoppanant, S. Y. Wong, P. Zhang, *Science* **2016**, *352*, 61–67; b) C. W. Coley, D. A. Thomas, J. A. M. Lummiss, J. N. Jaworski, C. P. Breen, V. Schultz, T. Hart, J. S. Fishman, L. Rogers, H. Gao, R. W. Hicklin, P. P. Plehiers, J. Byington, J. S. Piotti, W. H. Green, T. F. Jamison, K. F. Jensen, *Science* **2019**, *365*, eaax1566; c) A. Bédard, A. Adamo, K. C. Aroh, M. G. Russell, A. A. Bedermann, J. Torosian, B. Yue, K. F. Jensen, T. F. Jamison, *Science* **2018**, *361*, 1220–1225; d) S. Chatterjee, M. Guidi, P. H. Seeberger, K. Gilmore, *Nature* **2020**, *579*, 379–384; e) S. Steiner, J. Wolf, S. Glatzel, A. Andreou, J. M. Granda, G. Keenan, T. Hinkley, G. Aragon-Camarasa, P. J. Kitson, D. Angelone, L. Cronin, *Science* **2019**, *363*, eaav2211.
4. J. Workman, B. Lavine, R. Chrisman, M. Koch, *Anal. Chem.* **2011**, *83*, 4557–4578.
5. For reviews of PAT in continuous flow, see: a) B. J. Reizman, K. F. Jensen, *Acc. Chem. Res.* **2016**, *49*, 1786–1796; b) D. E. Fitzpatrick, C. Battilocchio, S. V. Ley, *ACS Cent. Sci.* **2016**, *2*, 131–138; c) S. Bordawekar, A. Chanda, A. M. Daly, A. W. Garrett, J. P. Higgins, M. A. LaPack, T. D. Maloney, J.

Morgado, S. Mukherjee, J. D. Orr, et al., *Org. Process Res. Dev.* **2015**, *19*, 1174–1185; d) T. Eifert, K. Eisen, M. Maiwald, C. Herwig, *Anal. Bioanal. Chem.* **2020**, *412*, 2037–2045; e) K. Eisen, T. Eifert, C. Herwig, M. Maiwald, *Anal. Bioanal. Chem.* **2020**, *412*, 2027–2035; f) G. A. Price, D. Mallik, M. G. Organ, *J. Flow Chem.* **2017**, *7*, 82–86; g) S. V. Ley, D. E. Fitzpatrick, R. J. Ingham, R. M. Myers, *Angew. Chem. Int. Ed.* **2015**, *54*, 3449–3464; h) J. J. Haven, T. Junkers, *Eur. J. Org. Chem.* **2017**, 6474–6482.

6. a) V. Sans and L. Cronin, *Chem. Soc. Rev.* **2016**, *45*, 2032–2043; b) A. D. Clayton, J. A. Manson, C. J. Taylor, T. W. Chamberlain, B. A. Taylor, G. Clemens, R. A. Bourne, *React. Chem. Eng.* **2019**, *4*, 1545–1554; c) C. Mateos, M. J. Nieves-Remacha, J. A. Rincón, *React. Chem. Eng.* **2019**, *4*, 1536–1544; d) M. Rubens, J. H. Vrijsen, J. Laun, T. Junkers, *Angew. Chem. Int. Ed.* **2019**, *58*, 3183–3187; e) M. Rubens, J. Van Herck, T. Junkers, *ACS Macro Lett.* **2019**, *8*, 1437–1441.
7. a) X. Duan, J. Tu, A. R. Teixeira, L. Sang, K. F. Jensen, J. Zhang, *React. Chem. Eng.* **2020**, 1751–1758; b) A. Pankajakshan, M. Quaglio, F. Galvanin, A. Gavriilidis, *React. Chem. Eng.* **2019**, *4*, 1623–1636.
8. a) J. S. Moore, K. F. Jensen, *Angew. Chem. Int. Ed.* **2014**, *53*, 470–473; b)B. M. Wyvratt, J. P. McMullen, S. T. Grosser, *React. Chem. Eng.* **2019**, *4*, 1637–1645; c) C. A. Hone, N. Holmes, G. R. Akien, R. A. Bourne, F. L. Muller, *React. Chem. Eng.* **2017**, *2*, 103–108.
9. M. G. Organ, J. S. Kwak, N. Bizarri, S. Sharif, D. Mallik, W. Zhang, *Chem. Eur. J.* **2020**, DOI 10.1002/chem.202003700
10. a) R. J. Ingham, C. Battilocchio, D. E. Fitzpatrick, E. Sliwinski, J. M. Hawkins, S. V. Ley, *Angew. Chem. Int. Ed.* **2015**, *54*, 144–148; b) D. E. Fitzpatrick, S. V. Ley, *Tetrahedron* **2018**, *74*, 3087–3100.
11. a) S. L. Lee, T. F. O'Connor, X. Yang, C. N. Cruz, S. Chatterjee, R. D. Madurawe, C. M. V. Moore, L. X. Yu, J. Woodcock, *J. Pharm. Innov.* **2015**, *10*, 191–199; b) C. J. Testa, C. Hu, K. Shvedova, W. Wu, R. Sayin, F. Casati, B. S. Halkude, P. Hermant, D. E. Shen, A. Ramnath, Q. Su, S. C. Born, B. Takizawa, S. Chattopadhyay, T. F. O'Connor, X. Yang, S. Ramanujam, S. Mascia, *Org. Process Res. Dev.* **2020**, DOI 10.1021/acs.oprd.0c00383; c) M. M. Nasr, M. Krumme, Y. Matsuda, B. L. Trout, C. Badman, S. Mascia, C. L. Cooney, K. D. Jensen, A. Florence, C. Johnston, K. Konstantinov, S. L. Lee, *J. Pharm. Sci.* **2017**, *106*, 3199–3206; d) A. Mesbah, J. A. Paulson, R. Lakerveld, R. D. Braatz, *Org. Process Res. Dev.* **2017**, *21*, 844–854.
12. P. Sagmeister, J. D. Williams, C. A. Hone, C. O. Kappe, *React. Chem. Eng.* **2019**, *4*, 1571–1578.
13. a) C. Vijaya Lakshmi, N. K. Katari, S. B. Jonnalagadda, *Green Process. Synth.* **2019**, *8*, 320–323; b) O. Ø. Thomsen, A. Cortot, D. Jewell, J. P. Wright, T. Winter, F. T. Veloso, M. Vatn, T. Persson, E. Pettersson, *N. Engl. J. Med.* **1998**, *339*, 370–374.
14. a) V. Hessel, D. Kralisch, N. Kockmann, T. Noël, Q. Wang, *ChemSusChem* **2013**, *6*, 746–789; b) V. Hessel, D. Kralisch, N. Kockmann, *Novel Process Windows: Innovative Gates to Intensified and Sustainable Chemical Processes*, Wiley-VCH, Weinheim, **2014**.
15. a) R. Lebl, Y. Zhu, D. Ng, C. H. Hornung, D. Cantillo, C. O. Kappe, *Catal. Today* **2020**, DOI 10.1016/j.cattod.2020.07.046; b) A. Avril, C. H. Hornung, A. Urban, D. Fraser, M. Horne, J. P. Veder, J. Tsanaktsidis, T. Rodopoulos, C. Henry, D. R. Gunasegaram, *React. Chem. Eng.* **2017**, *2*, 180–188; c) J. Gardiner, X. Nguyen, C. Genet, M. D. Horne, C. H. Hornung, J. Tsanaktsidis, *Org. Process Res. Dev.* **2018**, *22*, 1448–1452; d) C. H. Hornung, X. Nguyen, A. Carafa, J. Gardiner, A. Urban, D. Fraser, M. D. Horne, D. R. Gunasegaram, J. Tsanaktsidis, *Org. Process Res. Dev.* **2017**, *21*, 1311–1319.
16. a) C. J. Mallia, I. R. Baxendale, *Org. Process Res. Dev.* **2016**, *20*, 327–360; b) C. A. Hone, D. M. Roberge, C. O. Kappe, *ChemSusChem* **2017**, *10*, 32–41; c) H. P. L. Gemoets, Y. Su, M. Shang, V. Hessel, R. Luque, T. Noël, *Chem. Soc. Rev.* **2016**, *45*, 83–117.
17. a) D. Cantillo, M. Damm, D. Dallinger, M. Bauser, M. Berger, C. O. Kappe, *Org. Process Res. Dev.* **2014**, *18*, 1360–1366; b) D. Cantillo, B. Wolf, R. Goetz, C. O. Kappe, *Org. Process Res. Dev.* **2017**, *21*, 125–132; c) Y. Sharma, A. V. Nikam, A. A. Kulkarni, *Org. Process Res. Dev.* **2019**, *23*, 170–176; d) M. Köckinger, B. Wyler, C. Aellig, D. M. Roberge, C. A. Hone, C. O. Kappe, *Org. Process Res. Dev.* **2020**, *24*, 2217–2227.
18. L. Hohmann, S. K. Kurt, S. Soboll, N. Kockmann, *J. Flow Chem.* **2016**, *6*, 181–190.
19. For selected publications using membrane-based separators, see: a) A. Adamo, P. L. Heider, N. Weeranoppanant, K. F. Jensen, *Ind. Eng. Chem. Res.* **2013**, *52*, 10802–10808; b) C. Dai, D. R. Snead, P. Zhang, T. F. Jamison, *J. Flow Chem.* **2015**, *5*, 133–138; c) R. Lebl, T. Murray, A. Adamo, D. Cantillo, C. O. Kappe, *ACS Sustain. Chem. Eng.* **2019**, *7*, 20088–20096; d) A. J. Harvie, J. O. Herrington, J. C. Demello, *React. Chem. Eng.* **2019**, *4*, 1579–1588; e) L. Peeva, J. Da Silva Burgal, Z. Heckenast, F. Brazy, F. Cazenave, A. Livingston, *Angew. Chem. Int. Ed.* **2016**, *55*, 13576–13579; f) G. Y. Jeong, A. K. Singh, M. G. Kim, K. W. Gyak, U. J. Ryu, K. M. Choi, D. P. Kim, *Nat. Commun.* **2018**, *9*, 3968; g) R. A. Maurya, K. I. Min, D. P. Kim, *Green Chem.* **2014**, *16*, 116–120. See also, references 3a-c
20. P. Sagmeister, J. Poms, J. D. Williams, C. O. Kappe, *React. Chem. Eng.* **2020**, *5*, 677–684.
21. C. P. Holvey, D. M. Roberge, M. Gottsponer, N. Kockmann, A. Macchi, *Chem. Eng. Process.* **2011**, *50*, 1069–1075.
22. E. Mielke, D. M. Roberge, A. Macchi, *J. Flow Chem.* **2016**, *6*, 279–287.
23. a) S. Kern, K. Meyer, S. Guhl, P. Gräßer, A. Paul, R. King, M. Maiwald, *Anal. Bioanal. Chem.* **2018**, *410*, 3349–3360; b) S. Kern, L. Wander, K. Meyer, S. Guhl, A. R. G. Mukkula, M. Holtkamp, M. Salge, C. Fleischer, N. Weber, R. King, S. Engell, A. Paul, M. Pereira Remelhe, M. Maiwald, *Anal. Bioanal. Chem.* **2019**, *411*, 3037–3046.
24. a) J. R. Long, V. G. Gregoriou, P. J. Gemperline, *Anal. Chem.* **1990**, *62*, 1791–1797; b) F. Despagne, D. Luc Massart, *Analyst* **1998**, *123*, 157–178; c) J. Gasteiger, J. Zupan, *Angew. Chem. Int. Ed.* **1993**, *32*, 503–527.
25. To our knowledge, there is only a single recent report of NN processing for data generated by PAT in flow: S. Kern, S. Liehr, L. Wander, M. Bornemann-Pfeiffer, S. Müller, M. Maiwald, S. Kowarik, *Anal. Bioanal. Chem.* **2020**, *412*, 4447–4459.
26. For selected examples, see: a) D. C. Fabry, S. Heddrich, E. Sugiono, M. A. Liauw, M. Rueping, *React. Chem. Eng.* **2019**, *4*, 1486–1491; b) E. Fernandez-Puertas, A. J. Robinson, H. Robinson, S. Sathiyalingam, H. Stubbs, L. J. Edwards, *Org. Process Res. Dev.* **2020**, *24*, 2147–2156; c) A. Carangio, L. J. Edwards, E. Fernandez-Puertas, J. F. Hayes, M. M. Kucharski, G. W. Rutherford, K. M. P. Wheelhouse, G. D. Williams, *Org. Process Res. Dev.* **2020**, *24*, 1909–1915; d) T. Ouchi, C. Battilocchio, J. M. Hawkins, S. V. Ley, *Org. Process Res. Dev.* **2014**, *18*, 1560–1566.